Chemistry & Biology, Vol. 9, 1095–1107, October, 2002, ©2002 Elsevier Science Ltd. All rights reserved. PII S1074-5521(02)00239-9

Exclusive Interaction of the 15.5 kD Protein with the Terminal Box C/D Motif of a Methylation Guide snoRNP

Lara B. Weinstein Szewczak,[1,2] Suzanne J. DeGregorio,[1,2] Scott A. Strobel,[1,3] and Joan A. Steitz[1,2,4]

[1]Department of Molecular Biophysics and Biochemistry
[2]Howard Hughes Medical Institute
[3]Department of Chemistry
Yale University
New Haven, Connecticut 06536

Summary

Box C/D small nucleolar RNAs (snoRNAs) direct site-specific methylation of ribose 2′-hydroxyls in ribosomal and spliceosomal RNAs. To identify snoRNA functional groups contributing to assembly of an active box C/D snoRNP in *Xenopus* oocytes, we developed an in vivo nucleotide analog interference mapping procedure. Deleterious substitutions consistent with requirements for binding the 15.5 kD protein clustered within the terminal box C/D motif only. In vitro analyses confirmed a single interaction site for recombinant 15.5 kD protein and identified the exocyclic amine of A89 in box D as essential for binding. Our results argue that the 15.5 kD protein interacts asymmetrically with the two sets of conserved box C/D elements and that its binding is primarily responsible for the stability of box C/D snoRNAs in vivo.

Introduction

Maturation of eukaryotic ribosomal RNA (rRNA) requires modification of highly conserved rRNA sequences by covalent addition of methyl groups to specific ribose 2′-hydroxyls and the isomerization of specific uridines to pseudouridine [1]. In eukaryotes, box C/D snoRNPs participate in 2′-*O*-methylation [2–4] and box H/ACA snoRNPs in pseudouridylation of rRNAs (reviewed in [5] and [6]) as well as spliceosomal small nuclear RNAs U6 [7, 8] and U5 [9]. Archaeal species utilize related box C/D RNPs for rRNA 2′-*O*-methylation [10, 11].

The small nucleolar RNAs (snoRNAs) involved in ribose 2′-*O*-methylation are called methylation guide snoRNAs [8] to distinguish them from the minority of box C/D snoRNAs that facilitate cleavage events during rRNA biogenesis [12, 5]. Virtually all of the ~90 known mammalian methylation guide snoRNAs [13] contain four conserved sequence elements: boxes C (RUG AUGA) and D (CUGA) near the 5′ and 3′ termini, respectively, and internal copies of each box called C′ and D′ (Figure 1A). The mature 5′ and 3′ ends of many box C/D snoRNAs are sealed in a short stem [5], which together with boxes C and D forms the "terminal core motif" (Figure 1A; [14]). Each snoRNA has one or two regions of complementarity (10–21 nucleotides, nt) to rRNA that direct modification of the residue paired to the fifth nucleotide upstream of box D, D′, or both [5, 6].

SnoRNAs function within ribonucleoprotein particles. Core protein components of the box C/D snoRNPs are fibrillarin (Nop1p), Nop58p/Nop5p, Nop56p, and 15.5 kD (Snu13p) (reviewed in [15]). Fibrillarin is an abundant nucleolar protein (34 kDa) that has been implicated as the methyltransferase [16–19]. Although the stoichiometry of the box C/D particle is not known, some box C/D snoRNAs possess active guide sequences upstream of both boxes D and D′, supporting a model in which box C/D snoRNPs are comprised of two sets of the four core proteins, one set associated with each of the conserved box C/D motifs [20]. Similarly, box H/ACA snoRNPs are proposed to bind a set of four specific proteins to each of their two hairpin structures, creating a symmetric, bipartite particle [21].

Recent work identified the terminal core motif as a binding site for the human 15.5 kD (h15.5 kD) protein based on primary and secondary structural similarities between the box C/D snoRNAs and the 5′ stem-loop of U4 snRNA (shown for a consensus box C/D snoRNA in Figure 1A, right; [22, 23]). The 15.5 kD protein, a component of the U4 snRNP as well as box C/D snoRNPs, has been implicated as the factor allowing assembly of other U4 snRNP-specific proteins [24]. The same may be true for box C/D snoRNPs, as recently demonstrated in HeLa nuclear extracts (N.J. Watkins, A. Dickmanns, and R. Lührmann, submitted) and for *S. solfataricus* protein homologs in vitro [17]. Both the box C/D terminal motif [23] and the 5′ stem-loop of U4 [22, 25] conform to a general RNA structural motif termed the kink turn (K turn), found repeatedly in 23S rRNA [26] and prokaryotic mRNAs [27]. Two key features of this motif are the extrusion of a nucleotide between two stems to form the apex of a sharp kink and the presence in one stem of noncanonical base pairs, most frequently tandem sheared G-A pairs (see Figure 1A; [26, 25]). Since both boxes C/D and C′/D′ match the sequence consensus for a K turn, box C/D snoRNAs potentially contain two 15.5 kD binding sites.

In vivo, snoRNAs are matured by exonucleolytic trimming of longer precursors: intron sequences or independent transcription units [12, 5]. In yeast, 5′→3′ exonucleolytic trimming is carried out by Rat1p and 3′-end processing by the exosome (reviewed in [15]). Current models for snoRNP biogenesis suggest interplay between processing factors and the core proteins, which bind and protect the mature snoRNA sequences [15, 20]. Accordingly, mutations in box C, D, or the terminal stem destabilize snoRNAs in vivo (reviewed in [5] and [6]).

Nucleotide analog interference mapping (NAIM) uses nucleotide analogs to alter, delete, or add functional groups to specific positions in an RNA molecule [28]. Since the analogs are incorporated into a population of in vitro transcripts at all positions of the parent nucleotide, but an individual RNA contains only a single substitution, effects at each position can be simultaneously

[4]Correspondence: joan.steitz@yale.edu

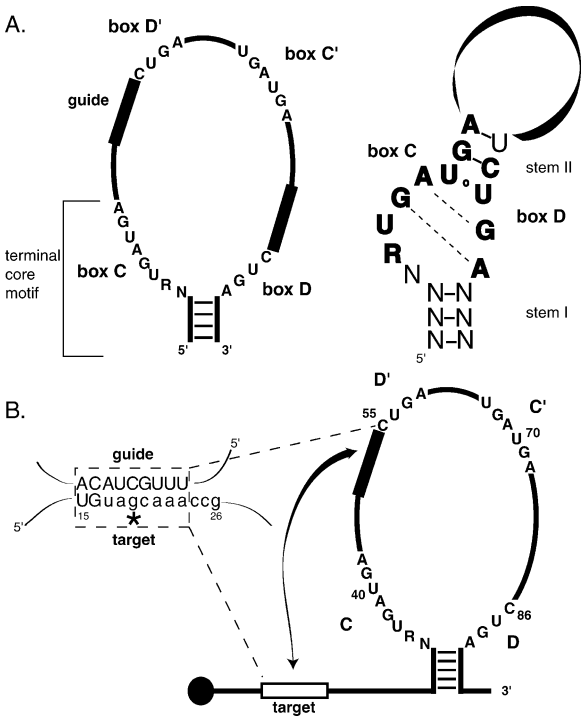

Figure 1. A Consensus Box C/D snoRNA Compared to the Composite snoRNA Constructed for This Study

(A) On the left, conserved features of the box C/D methylation guide snoRNAs are shown, including boxes C, C′, D, and D′, guide elements, and the terminal stem. On the right is the proposed secondary structure formed by boxes C and D, predicted by analogy to the U4 snRNA 5′ stem-loop [23]. Watson-Crick pairs are designated with solid lines, the two G-A pairs with dashed lines, and a U-U pair with an open circle. The 5′ U in box C corresponds to the extruded nucleotide in published structures of the kink-turn motif [26, 25].

(B) The composite snoRNA (complete sequence presented in Figure 6) bears a 5′ extension containing a sequence (target) complementary to the guide upstream of box D′. An enlarged view of the putative nine-base-pair duplex indicates G19, the designated site of 2′-*O*-methylation, with an asterisk. A unique RNase T_1 fragment produced after methylation at G19 is in lowercase letters. Sequences between boxes C′ and D (72–85) are from *Xenopus* U25 [4].

evaluated. Here we have used NAIM to identify RNA functional groups that contribute to box C/D snoRNP assembly in vivo in *Xenopus* oocytes. Most detected sites of interference clustered in boxes C and D, which form a binding site for the 15.5 kD snoRNP protein. One outlying interference in box D′ suggested the potential for a second binding site. However, in vitro binding and NAIM analyses confirmed the interaction of the 15.5 kD protein with only the terminal box C/D elements. More broadly, this study shows that NAIM can be used to study RNA functional group contributions in vivo.

Results

A Composite snoRNA that Assembles into a Stable snoRNP in *Xenopus* Oocytes

NAIM requires that active RNA molecules be selected from a population so that their functional groups can be compared with those of the unselected pool. We designed a box C/D snoRNA that could be selected based on its assembly into a snoRNP in *Xenopus* oocytes. One limitation of the NAIM approach is that nucleotides close to the ends of the RNA molecule are difficult to analyze [29]. To remedy this, we added sequence to the 5′ end of a conventional box C/D snoRNA and initiated transcription with a cap analog [A(5′)ppp(5′)G] to prevent exonucleolytic removal of the extension in vivo (Figure 1B). The 5′ extension contained a 9 nt target sequence for 2′-*O*-methylation to allow snoRNP function to be assessed. The RNA produced by in vitro transcription also extended beyond the terminal stem by 5–6 nt at the 3′ end. Since endogenous 3′-end-processing activity in *Xenopus* oocytes is known to degrade unassembled snoRNAs but trims correctly assembled snoRNAs to within a few nucleotides of the terminal stem [30, 31], an assay for snoRNP assembly was provided.

As shown in Figure 2A, the capped composite snoRNA was stable for 4 hr post nuclear injection (lane 9). As anticipated, the injected precursor transcript was trimmed only at the 3′ end (Figure 2A, compare lanes 2 and 9), which was stable for up to 24 hr (data not shown). The mature 3′ end was mapped (see Supplemental Data), confirming that the 3′ extension was reduced to 1–3 nt beyond the terminal stem (data not shown). Uncapped transcripts were processed to the 5′ end of the terminal stem (data not shown), consistent with their entry into the endogenous snoRNA biogenesis pathway. The stability of the trimmed composite snoRNA in vivo argues that proper assembly of protein factor(s) [32, 33] occurs in the *Xenopus* oocyte.

Fibrillarin is the hallmark protein associated with box C/D snoRNAs and enables their efficient immunoprecipitation by monoclonal antibody 72B9 [31, 34]. Body-labeled composite snoRNAs examined 4–7 hr after injection into *Xenopus* oocyte nuclei were immunoprecipitated by 72B9 (Figure 2A, lane 5) but not by an antibody to the spliceosomal Sm proteins (Y12) (lane 7). Primer extension analysis revealed equivalent efficiencies of 72B9 immunoprecipitation for the injected composite snoRNA (25%) and an endogenous methylation guide snoRNA (U28, 22%, data not shown). Since fibrillarin interacts only weakly with RNA transcripts in the absence of other proteins [35], these data argue that additional snoRNP proteins are bound.

The characteristic 3′-end trimming of assembled snoRNAs after 4–7 hr (Figures 2A and 3A, gray highlight) was exploited as the basis for selective 3′- end labeling in the subsequent NAIM analyses. SnoRNAs recovered from oocytes were labeled to produce a pool of homogeneous length by annealing a DNA splint that overlaps and extends beyond the 3′ end and filling in the 5′ overhang with α-^{32}P-dGTP and dATP (Figure 3A; [36]). As inaccurately or unprocessed RNAs are not extended, only those RNAs that are stable and have been correctly processed become labeled. Uninjected transcripts were similarly 3′-end labeled with α-^{32}P-dGTP using a DNA splint specific for the 3′ end resulting from T7 RNA polymerase (RNAP) transcription.

The Composite snoRNA Is Site Specifically Methylated In Vivo

The target sequence in our composite snoRNA is not homologous to any known cellular RNA, and 9 nt falls

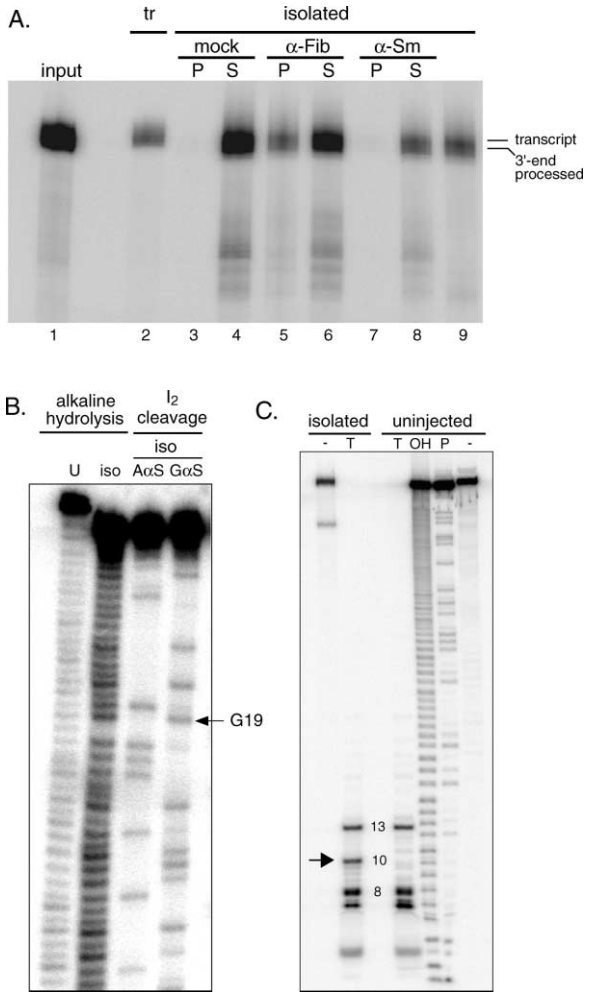

Figure 2. The Composite snoRNA Is Assembled, Processed, and Functional in the *Xenopus* Oocyte

(A) Body-labeled composite snoRNA (input, lane 1) was injected into *Xenopus* oocyte GVs. Following a 5 hr incubation, nuclei were manually isolated and either prepared for immunoprecipitation (lanes 3–8) or extracted to harvest total RNA (lane 9). Immunoprecipitations of 9–11 GVs were performed with beads alone (mock), anti-fibrillarin (α-Fib), or anti-Sm (α-Sm) antibodies. The total pellet (P) and supernatant (S) fractions were loaded. A dilution of the uninjected transcript RNA (tr) is shown (lane 2) for length comparison.

(B) Composite snoRNA was injected into *Xenopus* oocytes and 3′-end labeled following isolation (iso). It and the labeled uninjected transcript (U) were subjected to partial alkaline hydrolysis. G and A sequencing lanes were generated by I_2 cleavage of phosphorothioate-containing RNAs isolated from GVs.

(C) Total RNase T_1 digestion (T) of isolated body-labeled composite snoRNA produced a unique 10-mer (arrow) not present in the uninjected transcript. The smallest fragments produced by the digestion did not precipitate well. Thus, the 10-mer, resulting from methylation of G19, was easily detected, while the corresponding 3-mer and 7-mer were not visualized. The band intensities were quantified by PhosphorImager analysis. Partial alkaline hydrolysis (OH) and partial RNase T_1 (P) digests of 5′-end labeled uninjected transcript were compared to untreated RNA (-). Alkaline cleavage of 5′-end labeled RNA yields products with 5′- and 3′-phosphate termini, and consequently the small fragments (<10 nts) do not precisely comigrate with the products of RNase T_1 digestion.

below the thermodynamic threshold for formation of a productive intermolecular modification duplex [37]. Thus, the composite snoRNA should be modified only through formation of a self-target/guide duplex (shown for the *cis* reaction in Figure 1B). Two assays provided evidence that the injected RNA recovered from *Xenopus* oocytes was accurately and efficiently methylated.

Figure 2B shows a partial alkaline hydrolysis of 3′-end labeled isolated snoRNAs. A gap in the ladder immediately following G19, the site targeted for methylation, verified that a single site was methylated in the majority of the recovered, processed molecules.

The extent of modification was then determined by total RNase T_1 digestion of recovered versus uninjected transcripts (Figure 2C). Addition of a methyl group is predicted to block enzymatic cleavage at G19, leading to formation of a unique 10-nt-long fragment (Figure 1B, lowercase nucleotides; Figure 2C, arrow). Its quantification relative to the largest fragment, a 13-mer, revealed 85% modification.

We did not further investigate whether methylation occurs in *cis* or *trans*, as this distinction does not affect the conclusion that an active particle has been assembled. We conclude that the composite snoRNA entered the endogenous snoRNP biogenesis pathway as evidenced by its accurate processing and assembly with specific proteins to form functional particles.

NAIM Analysis of In Vivo Assembled snoRNAs

We analyzed snoRNP biogenesis by identifying sites where functional group substitution impairs particle assembly, leading to degradation of the altered snoRNAs. In vitro transcriptions were performed with a nucleotide analog α-thiotriphosphate (NTPαS) concentration sufficient to produce roughly one substitution per molecule [28]. This created a pool of RNAs, each bearing a substitution at a different position, with every position sampled within the pool (illustrated for a hypothetical U analog, δTPαS, in Figure 3A). The thiophosphate linkage (sulfur substitution of the pro R_P-oxygen) both serves as a tag for the incorporated nucleotide and tests for backbone interactions (Figure 3B). After particle assembly within the *Xenopus* oocyte, isolated snoRNA was 3′-end labeled, cleaved by addition of I_2, and its sequencing ladder compared with that of uninjected RNA (Figure 3B).

Quantitative analysis measured the extent of interference by a nucleotide alteration, normalized both for the incorporation of the analog at each particular position (derived from quantification of the uninjected transcript ladder) and for loading differences between lanes. Designated kappa (κ), this normalized value compares the effects of different functional group substitutions [28]. Error bars in Figures 3B and 4B indicate variability, with values for samples injected on the same day differing less than those for the same RNA transcript injected on different days.

An In Vivo Phosphorothioate Effect in Box C

In contrast to conventional mutagenesis approaches, NAIM can identify backbone atoms important for snoRNP stability and assembly. Analysis of the recovered composite snoRNAs containing U, C, G, or AαS

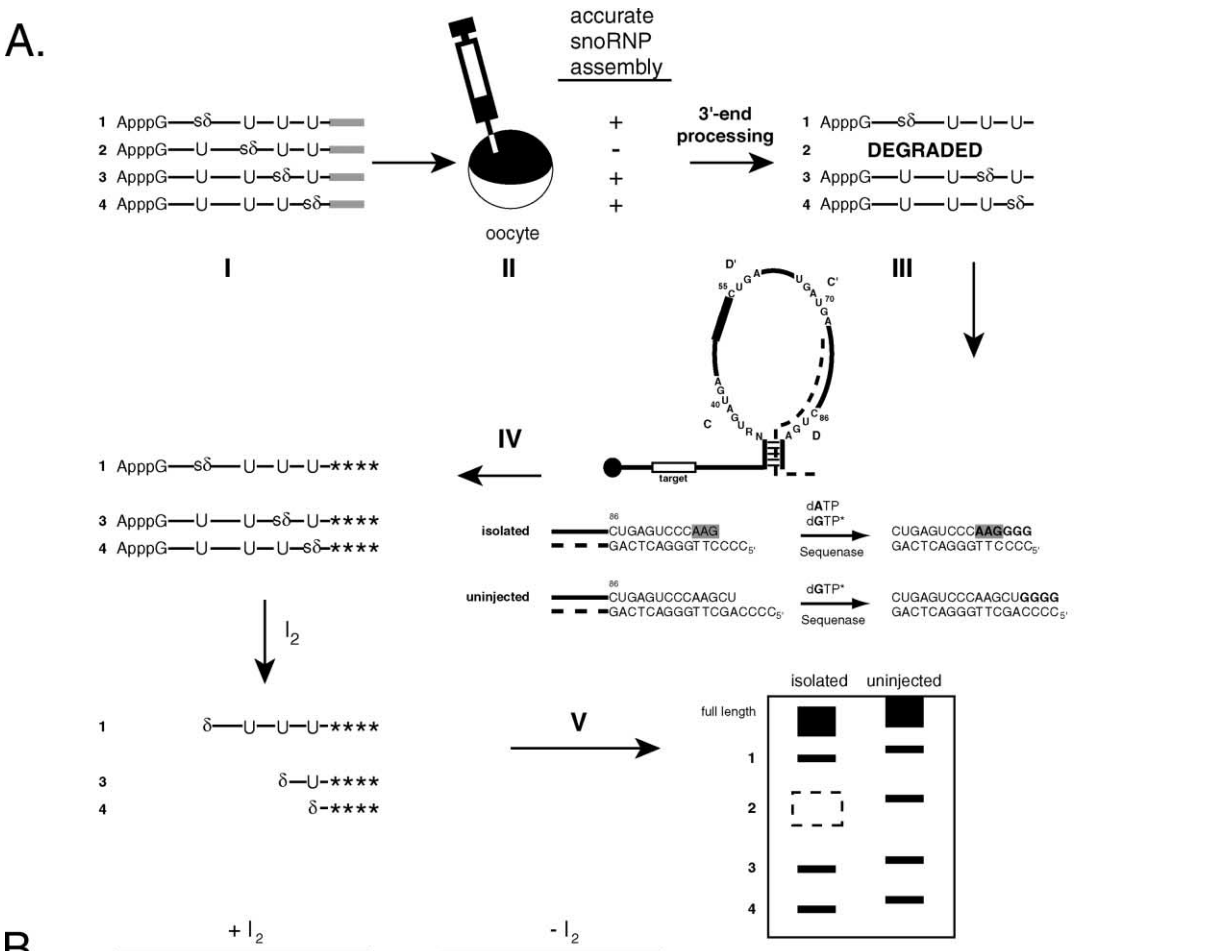
A.
accurate
snoRNP
assembly
3'-end
processing
DEGRADED
oocyte
I
II
III
IV
V
target
isolated
uninjected
dATP
dGTP*
Sequenase
full length
isolated
uninjected

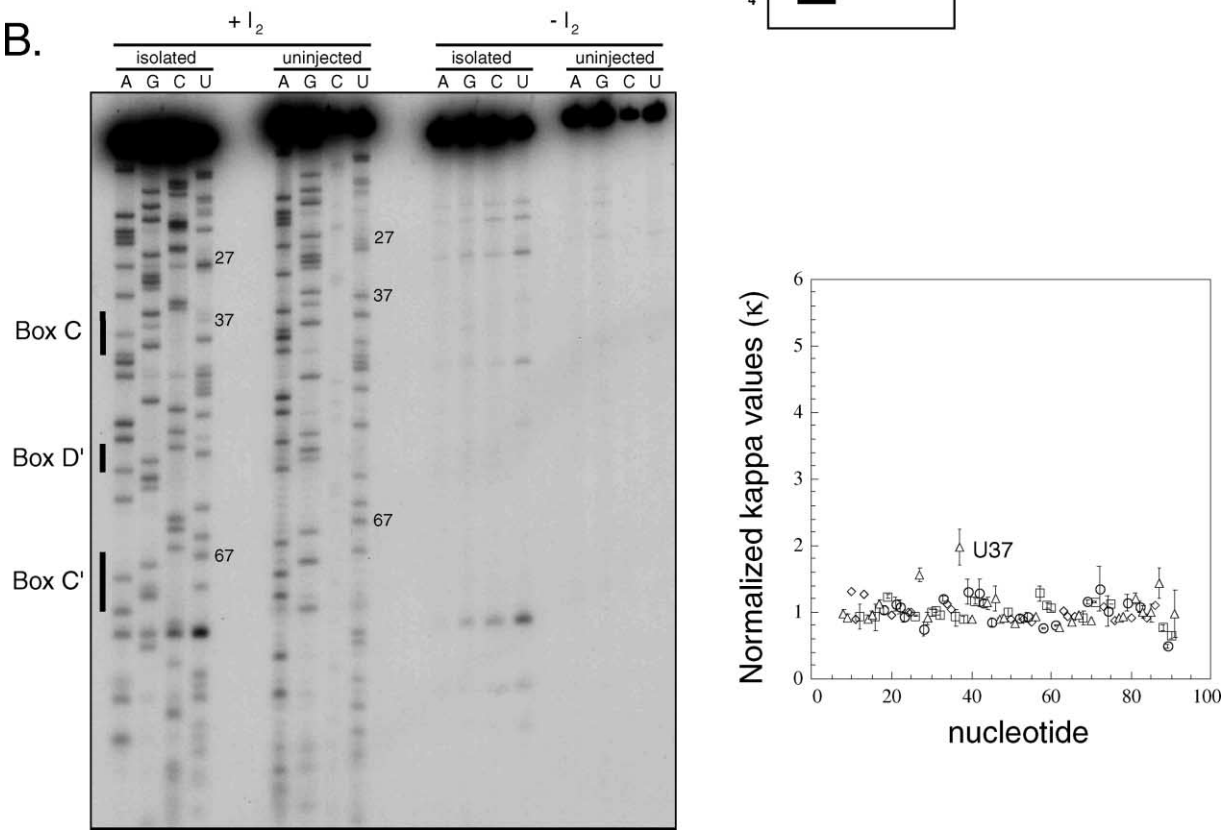
B.
+ I2
- I2
isolated
uninjected
A G C U
Box C
Box D'
Box C'
27
37
67
Normalized kappa values (κ)
U37
nucleotide

revealed a single strong site of phosphorothioate interference at position 37 (shown in Figure 3B for UαS). U37 is located in the conserved box C element (R**pU**GAUGA) and is predicted to be the extruded nucleotide in the K-turn structure (Figure 1A). Lesser effects were observed at U27 in the 5′ extension and U87 in box D (C**pU**GA, see Figure 3B).

To examine ribose functional groups, analogs modified at the 2′ position were incorporated into chimeric snoRNA transcripts using a mutant T7 RNAP [28, 38]. SnoRNAs containing 2′-deoxyuridine, 2′-deoxyadenosine, 2′-deoxyguanosine, or 2′-deoxy, 2′-fluorouridine showed no reproducible sites of interference.

Base Interactions Important for snoRNP Assembly In Vivo Reside in Three of the Conserved Box Elements

Guanosine residues occur at conserved positions in each of the box elements. Inosine (Figure 4A, IαS), a guanosine analog lacking the exocyclic amine, yielded a single position of clear interference at G38 (Figure 4B) in box C (RU**G**AUGA). Comparable positions in the U4 5′ stem-loop and a U14 snoRNA fragment have been shown by conventional mutagenesis to be essential for binding the h15.5 kD protein [22, 23].

Several analogs of adenosine (Figure 4A) were investigated for their effects on snoRNP assembly. 2,6-diaminopurine (DAPαS), which adds an extra exocyclic amine to the base's Watson-Crick face, did not impair assembly at any position within the composite snoRNA (Figure 4B). In contrast, N6-methyladenosine ($m^6A\alpha$S) and purine riboside (PurαS), both of which alter the exocyclic amine of A, did. Removing the exocyclic amine entirely, PurαS produced interference at positions 39, 58, and 89 in box C (RUG**A**UGA), box D′ (CUG**A**), and box D (CUG**A**) (Figure 4B, open diamonds), respectively. Addition of a methyl group ($m^6A\alpha$S, blocking one hydrogen bond donor and adding steric bulk) likewise caused interference, although of lower magnitude, at positions 39 and 58 (black squares).

Finally, two analogs of uridine, pseudouridine ($\psi\alpha$S) and 5-methyluridine ($m^5U\alpha$S), did not produce any sites of interference in the chimeric snoRNA molecule.

In Vitro Analyses Indicate Binding of Recombinant h15.5 kD to Only Boxes C and D

Five of the seven functional groups contributing to snoRNP assembly in vivo (Figures 3 and 4) lie within the terminal C and D boxes, the documented binding site for the 15.5 kD core protein (Figure 1A; [39, 23]). Since boxes C′ and D′ have the potential to form a comparable binding site, the single interference we observe in box D′ (A58) could result from a second interaction with that protein, consistent with current models [20]. We tested this possibility by examining the binding of 15.5 kD to the composite snoRNA directly. Recombinant human 15.5 kD was expressed in *E. coli* as a glutathione-S-transferase (GST) fusion protein (the plasmid was a gift from R. Lührmann), and the GST tag was removed by cleavage with thrombin (see Supplemental Data). The 15.5 kD protein is highly conserved across species [39, 22], and the human protein is anticipated to bind the composite snoRNA in a manner akin to its *Xenopus* homolog (92% identity, GenBank Accession Number BF427309).

A gel mobility shift assay was employed to separate the 15.5 kD-snoRNA complex (RNP) from free RNA (Figure 5A, lanes 1–3 and 7–9; Supplemental Data Figure S1). Addition of progressively larger amounts of protein resulted in complete binding of the trace radiolabeled RNA ($<$1 nM), with an apparent dissociation constant of 130 nM (data not shown). This value is $\sim$15-fold higher than that reported for U14 [23] and $\sim$25-fold higher than the upper limit reported for the terminal core motif alone [39], and may be due to differences arising from the lack of boxes C′ and D′ in U14 and its derivatives, differences in the methods used to determine the values (Kuhn et al. utilized filter binding), or the presence of a 5′ extension on our composite snoRNA. Importantly, over the range of concentrations tested, only a single shifted complex was observed. A *Xenopus* snoRNA, U25 [4] (K_d = 90 nM), and a modified human snoRNA, U75 [40], bound similarly in vitro (J.S. Gabrielsen, L.B.W.S., and J.A.S., unpublished results).

NAIM results (Figure 4) indicated that purine substitution in box D (A89) impaired snoRNA stability, potentially by disrupting binding of the *Xenopus* 15.5 kD protein. This analog was therefore exploited to ask whether 15.5 kD binds in vitro to both box C/D motifs. Composite RNAs bearing an A-to-Pur change in either box D′ (A58Pur) or box D (A89Pur) were constructed by DNA-mediated RNA ligation [41]. Binding of the purine-containing RNAs to the recombinant h15.5 kD protein was compared to wild-type RNA, also generated by ligation (Figure 5A). Removal of this single amine from box D abolished interaction (Figure 5A, lanes 10–12), whereas substitution in box D′ had no effect (lanes 4–6). If the shifted complex resulted either from highly cooperative binding of h15.5 kD to the two sets of box elements or

Figure 3. NAIM Analysis of In Vivo Assembled, Processed snoRNAs

(A) Schematic of the NAIM procedure. (I) A pool of capped RNA transcripts containing a phosphorothioate-tagged nucleotide analog incorporated on average once per molecule (shown for a U analog, sδ) was injected (II) into the nuclei of *Xenopus* oocytes, where assembly with snoRNP proteins and 3′-end processing (III, sequences removed by processing shown as gray bars) occur. After isolation of nuclear RNA, the 3′-trimmed composite snoRNAs were 3′-end labeled (IV) by annealing a sequence-specific DNA splint (dashed line), which creates a 5′ overhang, and filling in with α-^{32}P-dGTP and dATP. Treatment with I_2 hydrolyzed the phosphorothioate linkages, and the resulting fragments were resolved by denaturing PAGE (V). If functional group substitution impairs snoRNP assembly, the RNA is degraded, resulting in a gap in the sequencing ladder as compared to the uninjected pool (labeled as described in Experimental Procedures).

(B) Phosphorothioate interference at U37 in box C (RpUGAUGA). Interference values (κ) plotted against the nucleotide position within the composite snoRNA. Values are considered significant if they are reproducibly above background. Standard errors of the mean are shown for AαS (circles, n = 3), GαS (squares, n = 2), and UαS (triangles, n = 7). CαS is shown with diamonds. Similar results were obtained 16 hr after injection into oocytes.

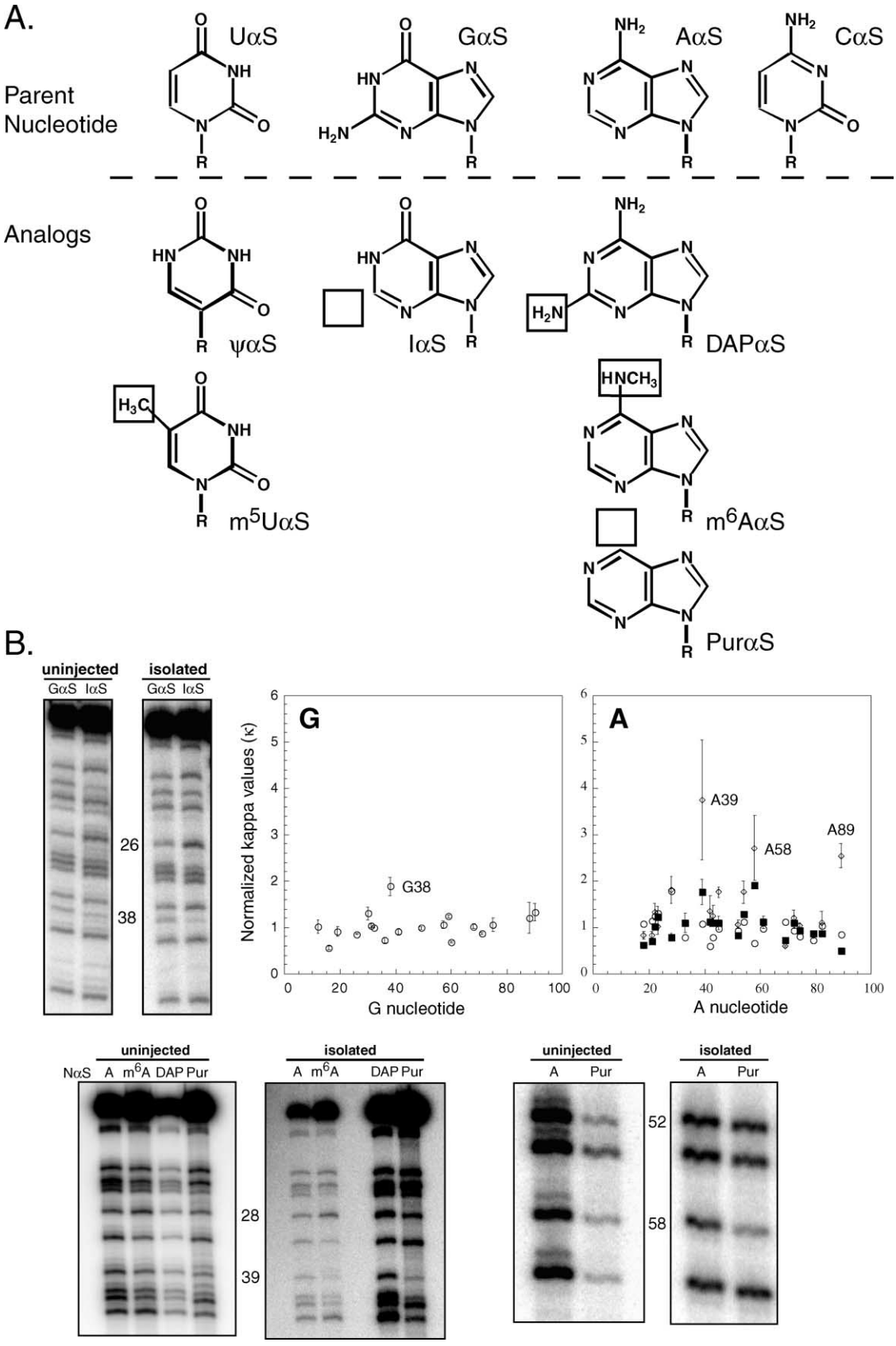

Figure 4. Interference Produced by Base Analogs

(A) Base analogs examined. Functional group changes are boxed.

(B) Interference by substitution with base analogs. Inosine (IαS) caused interference in box C (RUGAUGA). 2,6-dimethyladenosine (DAPαS, open circles), N6-methyladenosine (m^6AαS, closed squares), and purine (PurαS, open diamonds) are compared to adenosine (A). Interference values (κ) are plotted against the nucleotide position within the composite snoRNA, with standard errors of the mean shown for **G**, IαS (n = 4); **A**, m^6AαS (n = 3); and PurαS, (n = 4).

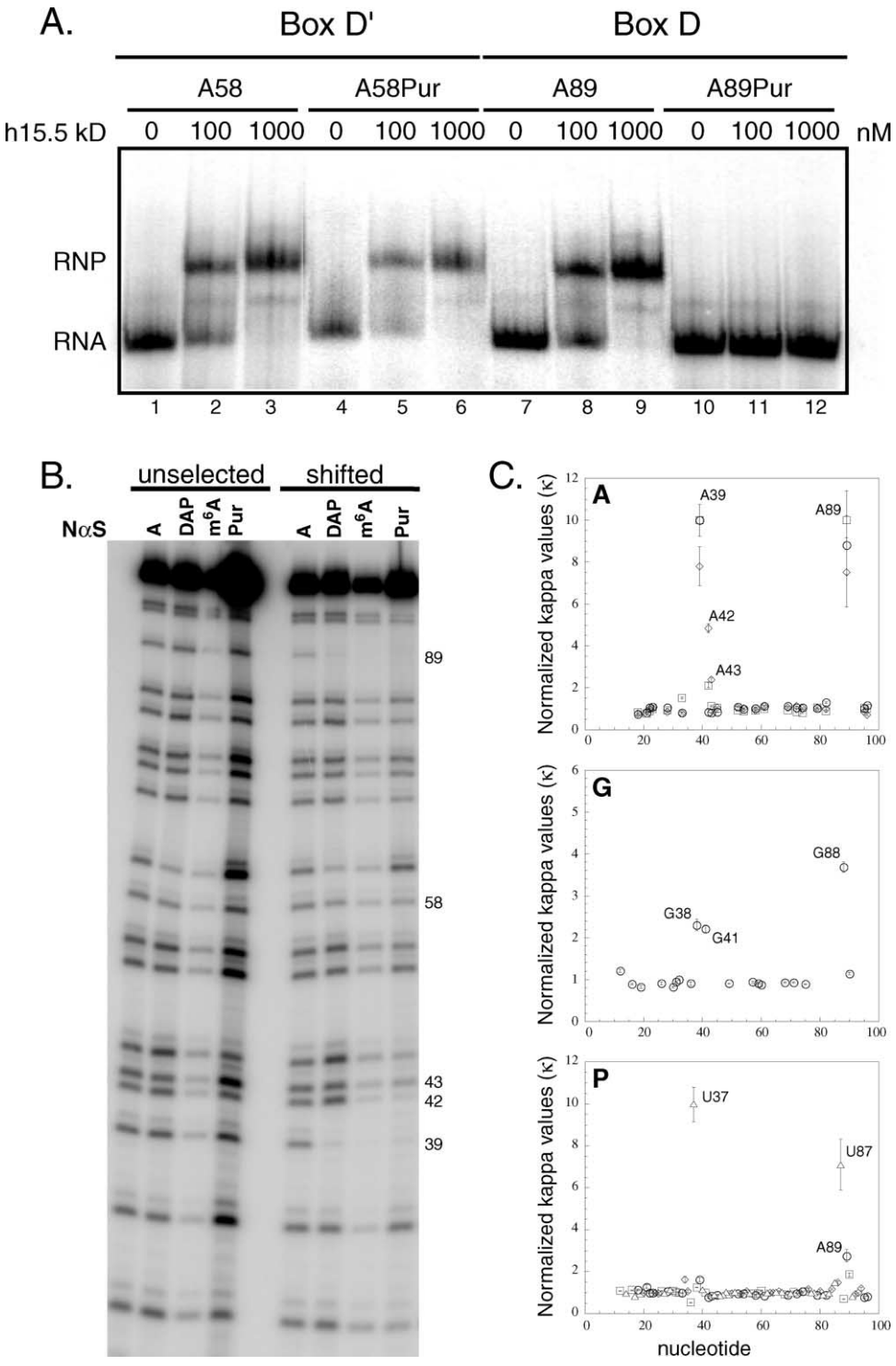

Figure 5. Recombinant h15.5 kD Binds the Composite snoRNA In Vitro via Essential Functional Groups in Boxes C and D Only

(A) RNAs with a purine substitution in box D′ (A58Pur) or box D (A89Pur) or the wild-type sequence (A58 and A89) were incubated with recombinant h15.5 kD for 1 hr at 4°C. The RNA-protein complex (RNP) was separated from the free RNA (RNA) by 8% nondenaturing PAGE (80:1 acrylamide:bisacrylamide).

(B) Transcripts containing AαS, DAPαS, m^6AαS, or PurαS were selected by h15.5 kD binding and compared to unselected RNAs after treatment with I_2 and resolution on 10% denaturing PAGE.

(C) Interference values (κ) plotted against nucleotide position within the snoRNA. Standard errors of the mean are shown for **A:** DAPαS (circles, n = 4), m^6AαS (squares, n = 4), PurαS (diamonds, n = 4); **G:** IαS, n = 4; **P:** AαS (circles, n = 4), GαS (squares, n = 6), CαS (diamonds, n = 2), and UαS (triangles, n = 4).

from stochastic binding to either box D or D′, substitutions in either box should at least partially disrupt complex formation. We conclude that the 15.5 kD protein binds only to the motif formed by boxes C and D, and that binding depends critically on the presence of the exocyclic amine of A89 in box D.

NAIM Reveals Conserved Functional Groups in Boxes C and D Essential for 15.5 kD Binding In Vitro

To determine if the in vivo interference pattern could be ascribed solely to 15.5 kD binding, we used analog-substituted snoRNA transcripts labeled at their 5′ ends in a gel shift selection to identify functional groups contributing to RNP formation in vitro. Recombinant h15.5 kD protein was added to the reactions at a concentration (117 nM) close to the measured K_d to create a competitive selection for protein binding (40%–60% binding was observed in each selection). After incubation at 4°C for 1 hr, the bound RNAs were separated from the unbound on nondenaturing gels. The RNP band RNAs were then compared to the unselected pool, and interference values (κ) were calculated (Figure 5C).

As visualized in Figure 5B, alteration of the adenine bases in the terminal box C/D motif disrupted binding of the 15.5 kD protein. At position 39 in box C (GUG**A**UGA), addition of an N2 exocyclic amine (DAPαS) or alteration of the N6 exocyclic amine (m^6A or PurαS) strongly impaired association, as did removal or methylation of the exocyclic amine of A42 (GUGAUG**A**). PurαS incorporation at A43, immediately following box C, also interfered with binding. As observed for A39 in box C, A89 in box D (CUG**A**) was sensitive to substitution with all analogs tested, recapitulating the binding defect seen with A89Pur (Figure 5A). In striking contrast, no sites of interference were detected in either box C′ or box D′ (Figures 5B, 5C, and 6).

Alteration of the conserved Gs in boxes C and D was also deleterious to h15.5 kD binding (Figure 5C). Removal of the exocyclic amine by incorporation of IαS resulted in three sites of interference: G39 and G41 in box C (GU**G**AU**G**A) and G88 in box D (CU**G**A). These effects are consistent with the involvement of G39 and 88 in sheared G-A pairs and with G41 forming a Watson-Crick pair in stem II of a kink turn (Figure 1A).

Finally, three phosphate oxygens were observed to contribute to complex formation (Figure 5C). Replacement of U37 in box C (G**pU**GAUGA) and U87 in box D (C**pU**GA) with UαS strongly destabilized h15.5 kD interaction, as did AαS incorporation in box D (CUG**pA**). Interestingly, replacing the R_P-oxygen with sulfur at position 36 in box C (**pG**UGAUGA) reproducibly enhanced (κ ~0.5) binding of the composite snoRNA to the protein. We conclude that, in vitro, h15.5 kD interacts with the snoRNA nucleotide bases and backbone only in boxes C and D (Figure 6).

Discussion

To identify individual functional groups essential for box C/D snoRNP assembly in vivo, we performed a NAIM analysis using a composite snoRNA with an extended

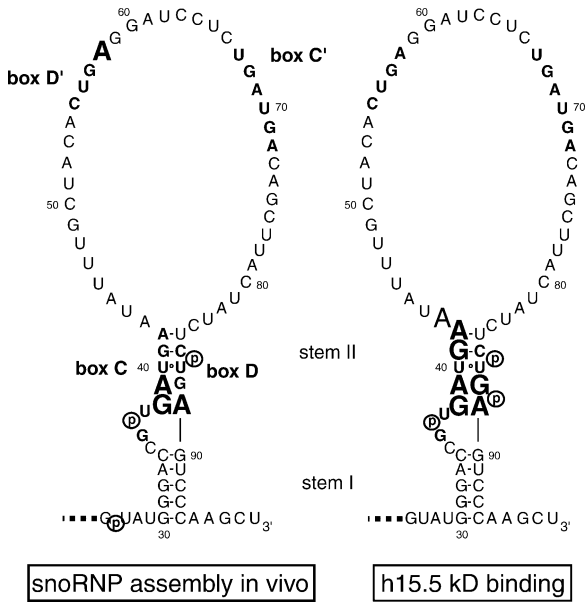

Figure 6. Summary of Interference Data for Composite Box C/D snoRNP Assembly

On the left, the observed sites of interference derived from in vivo selection for assembly, stability, and 3′-end processing in *Xenopus* oocytes are shown on a hypothetical secondary structure for the composite snoRNA. Sites of phosphorothioate interference are circled; positions of base analog interference are in large type; nucleotides in the conserved box elements are in bold. The sequence of the first 25 nts of the composite snoRNA (- - -) is 5′-GGGCGAAUUC CGCUUGUAGCAAACC-3′. On the right, observed sites of interference derived from in vitro selection for binding by recombinant h15.5 kD are shown.

sequence upstream of a consensus box C/D snoRNA. Upon injection into *Xenopus* oocytes, the composite snoRNA was assembled into mature, functional particles as judged by prolonged RNA stability, accurate 3′-end processing, association with fibrillarin, and efficient 2′-*O*-methylation. NAIM identified functional groups important for snoRNP assembly in vivo residing primarily but not exclusively within the snoRNA terminal box C/D motif (Figure 6). The in vivo interference patterns observed for nucleotides U37, G38, A39, U87, and A89 of our composite snoRNA correlate remarkably well with contacts made in the U4 fragment/h15.5 kD structure ([25]; see Figure 7, key functional groups shown as enlarged balls) and with the conserved features of the K turn [26]. Together with in vitro binding and NAIM results, our data suggest a model for snoRNP assembly in which a single 15.5 kD protein binds a K-turn structure assumed by the terminal box C/D motif to nucleate particle formation.

The 15.5 kD Protein Binds Boxes C/D but Not C′/D′

SnoRNA boxes C′ and D′ have the same consensus sequences [42] and in our composite snoRNA are identical to boxes C and D (Figure 1). Therefore, they can potentially adopt the same structure as boxes C and D. Although the overall sequence conservation is less than observed for boxes C and D [14], the GA dinucleotides

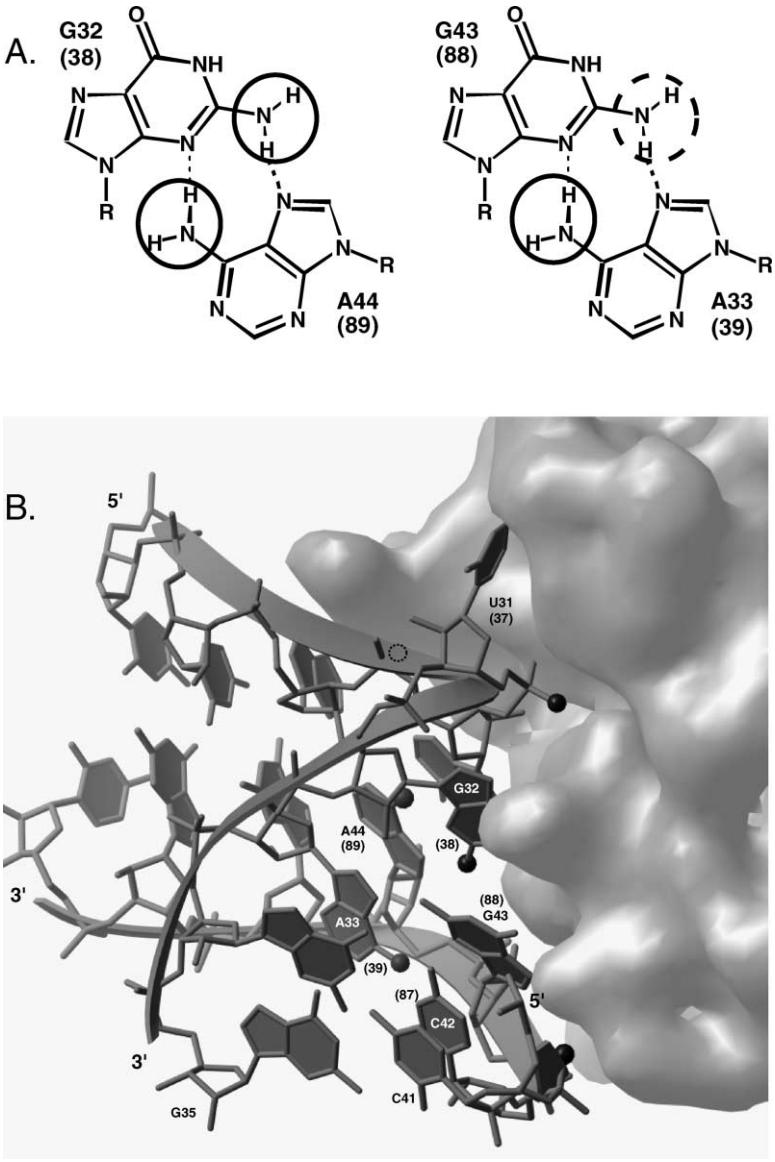

Figure 7. Structural Context for the Important snoRNA Functional Groups Identified by NAIM

(A) Functional groups identified by NAIM (circled) establish formation of two sheared G-A pairs in vivo. Pairing geometry was taken from the U4 snRNA stem-loop structure [25], with the additional exocyclic amine identified only in vitro shown with a dashed circle. The base pairs are labeled with respect to U4 (composite snoRNA numbering in parentheses).

(B) RNA functional groups (U4 numbering, snoRNP numbers in parentheses) identified as important for in vivo snoRNP assembly [R_P oxygens of U31 (37) and C42 (U87) phosphates, N2 of G32 (38), N6 of A33 (39) and N6 of A44 (89)] are marked with large balls (black for RNA-protein interactions and gray for RNA-RNA contacts) on the X-ray crystal structure of U4 snRNA 5′-stem loop and h15.5 kD [25]. The R_P-oxygen of A30 (equivalent to G36) is obscured by the ribbon backbone but is indicated by a dashed circle. Only the surface of the 15.5 kD protein is shown. The cross-strand purine stack involves A30 (G36), A44 (89), and A33 (39) [25].

required to form the G-A pairs at the heart of the K turn are each 94% conserved for G and A in box D′ and 77% and 68% conserved for the G and A, respectively, in box C′ [42]. Indeed, Omer and coworkers [17] concluded that the archaeal homolog of 15.5 kD, aL7a, can bind to both boxes C/D and C′/D′ in vitro.

In contrast, our results both in vivo (Figures 3 and 4) and in vitro with either singly substituted RNAs (Figure 5A) or populations of substituted RNAs (Figures 5B and 5C) argue against interaction of the 15.5 kD protein with boxes C′ or D′. Yet, since the guide sequence upstream of box D′ is functional in methylation (Figure 2A), the methyltransferase (fibrillarin) must assemble onto box D′ of the composite snoRNA even in the absence of 15.5 kD binding. Accordingly, crosslinking results with another functional box C/D snoRNP [43] demonstrated that the position of the guide sequence does not affect the protein interactions within the particle. We conclude that the single site for 15.5 kD binding is likely a general feature of box C/D snoRNPs involved in methylation.

Correlation of Functional Groups Important for 15.5 kD Binding In Vivo and In Vitro

Interference by IαS, m^{6}AαS, and PurαS provides experimental support for the formation of a kink-turn structure by the terminal box C/D motif of our composite snoRNA (Figures 6 and 7A). Specifically, removal of the exocyclic amines of G38 and A89 would disrupt hydrogen bonding in the first sheared G-A pair (Figure 7A), while interference upon methylation or removal of the exocyclic amine of A39 is consistent with formation of the second G-A pair of a K turn (Figure 4). Although apparent only in vitro, IαS interference at G88 (Figure 5C) establishes it as a participant in the second G-A pair. These results argue that h15.5 kD binds to a K turn formed by the terminal box C/D motif both in vivo and in vitro.

While the bases now known to be involved in the 15.5 kD binding interaction had been previously identified (reviewed in [5] and [6]), NAIM analysis uncovered backbone contributions to RNP formation (Figures 3 and 5C). Both in vivo and in vitro, replacement of U37's

phosphate with a phosphorothioate disrupted interactions (Figures 3 and 6). U37 corresponds to U31, the extruded nucleotide in the U4 snRNA fragment (Figure 7B), whose phosphate oxygen is integral to the protein-RNA interface and makes a direct hydrogen bond to the backbone amide of Ala-39 [25]. Thus, it seems likely that substitution of the pro-R_P oxygen with sulfur at position 37 in box C prevents h15.5 kD and its *Xenopus* homolog from binding to the terminal core motif of the snoRNA in vitro and in vivo, respectively.

Surprisingly, the binding of recombinant h15.5 kD protein was strongly inhibited by an A-to-purine change in box D. Although A-to-C mutants had previously been shown to interfere with 15.5 kD binding [39, 22, 23], the change to purine is comparatively subtle. In the X-ray crystal structure of h15.5 kD bound to a fragment of U4 (Figure 7), the adenosine equivalent to A89, A44, does not interact directly with the protein [25]; rather, it participates in an cross-strand purine stacking interaction (Figure 7B) and donates a hydrogen bond to N3 of G32 in a sheared G-A pair (Figure 7A). Purine substitution should maintain stacking [44], suggesting that the binding defect is due instead to loss of hydrogen bonding. This argues that the RNA structure forms in the absence of protein (consistent with thermal melting studies of a truncated snoRNA [39]) and that the correct RNA conformation is essential for protein binding. In the 50S ribosome, K turns are bound in diverse ways by proteins with homologous RNA binding domains [26]. We predict that all such protein-RNA interactions would be similarly affected by this single functional group change. Perhaps the internal location of the C′/D′ motif renders it unable to preform the K turn and therefore unable to bind the 15.5 kD protein.

Despite substantial overlap, the NAIM patterns in vivo and in vitro were not identical even within the terminal core motif. Perhaps because of greater sensitivity, more functional groups were detected in vitro (Figure 6), for example G41 and A42 in conserved stem II (Figures 1, 5B, and 5C). Alternatively, assembly of additional proteins onto the snoRNP in vivo may diminish the energetic contributions of these functional groups. The phosphorothioate enhancement (position 36, Figure 5C) observed for the conserved purine nucleotide in box C (**pG**UGAUGA) in vitro was not expected. In structural models for the K turn [26, 25], the pro-R_P oxygen interacts electrostatically with the protein (dashed circle in Figure 7). Since the electrostatic character of a phosphorothioate differs from a phosphate in that the negative charge associated with the nonbridging atoms localizes to the sulfur [45], phosphorothioate substitution may enhance electrostatic interaction with the protein.

Implications for snoRNP Biogenesis

Our analysis of functional groups required for in vivo snoRNP assembly supports a model [24] in which snoRNP assembly begins with binding of the 15.5 kD protein to the terminal box C/D motif. In vitro analyses of snoRNP assembly are also consistent with the human 15.5 kD protein (N.J. Watkins, A. Dickmanns, and R. Lührmann, submitted) or its archaeal homolog [17] binding first. The clustering of interferences within its binding site implicates 15.5 kD as the protein primarily responsible for particle stability and suggests that if it does not bind, other proteins may not associate, or if they do, they are not sufficient to prevent RNA degradation.

The interference we observe within the internal D′ box element at A58 was completely unanticipated (Figure 5), since previous analyses of box D′ mutations did not show any impact on particle stability [46, 47, 42]. As interaction with 15.5 kD seems unlikely, the internal C′/D′ motif may interact with other box C/D core proteins. A recent site-specific crosslinking analysis of a functional methylation guide snoRNP in *Xenopus* oocytes revealed binding of Nop58p to box C only, Nop56p to box C′, and fibrillarin to boxes D, D′, and C′, but not C [43]. Hence, either Nop56p or fibrillarin may interact with A58 in box D′. In yeast, Nop56p is not required for the stability of the box C/D snoRNA population and its association with snoRNAs requires fibrillarin, which in turn is linked to stability of snoRNAs released from introns and accurate end formation [33]. However, similar properties for the vertebrate proteins remain to be demonstrated. Alternatively, another RNA functional group may be interacting with the exocyclic amine of A58.

Significance

Box C/D snoRNAs assemble via an unknown pathway with four core proteins to form functional RNPs. Our results argue that the 15.5 kD protein interacts with only one of the two sets of conserved box C/D elements and that its binding is primarily responsible for the stability of box C/D snoRNAs in vivo. Microinjection of RNA pools into *Xenopus* oocytes now extends the application of NAIM into living cells. In a composite box C/D snoRNA, functional groups involved in RNA-RNA interactions as well as protein-RNA interactions were identified. These results provide in vivo validation for extending conclusions derived from the X-ray crystal structures of protein-bound kink turns to box C/D snoRNPs. Such an application of NAIM is well suited to the study of many RNPs and can potentially allow direct correlation of structural features with assembly and biological function.

Experimental Procedures

Supplemental Data

The following information and procedures can be found in the Supplemental Data: a description of the composite snoRNA sequence, oligonucleotide sequences, plasmid construction, RNA transcription, RNA 3′-end mapping, immunoprecipitations, and protein expression and purification. Please write to chembiol@cell.com for a PDF.

Nucleotide Analog Incorporation

Transcriptions to incorporate nucleotide analogs were performed in 100–200 μl using nucleoside α-thiotriphosphate and parent NTP ratios designed to achieve ~5% thiophosphate incorporation as described [28]. For incorporation of GTPαS, ITPαS, and dGTPαS, the published concentrations were decreased 10-fold to accommodate the reduced GTP concentration used in transcriptions containing A(5′)ppp(5′)G.

Xenopus Oocyte Manipulation and Nuclear RNA Preparation

Late stage V or stage VI oocytes were manually isolated from ovary tissue and stored prior to injection in OR3 medium at 18°C for a

maximum of 24 hr [48]. Nine or 13.8 nl of the RNA transcript (0.2–5 μM) was injected into the germinal vesicles (GVs) of 30 to 60 oocytes. After incubation at 18°C for either 4–7 hr or overnight, GVs were isolated manually in phosphate buffer with magnesium [49], immediately transferred with minimal buffer to dry ice, and stored at −80°C. Total nuclear RNA was prepared [50] from GVs digested in proteinase K buffer (30 μl/GV: 50 mM Tris-HCl [pH 7.6], 5 mM EDTA, 1.5% sodium dodecylsulfate, 300 mM NaCl, and 1.5 mg/ml proteinase K [AMRESCO]).

Analysis of 2′-*O*-Methylation

Ribonuclease T_1 Analysis

Nine nanoliters of purified composite snoRNA containing α-^{32}P-CTP (0.15 μM) was injected per oocyte. After 18 hr at 18°C, total nuclear RNA was prepared and dissolved to yield 2 GV equivalents per microliter. For the uninjected control, the radiolabeled transcript was mixed with 3 GV equivalents of *Xenopus* nuclear RNA prior to digestion. Digestion reactions (10 μl containing 4–8 GV equivalents) were performed in 4 M urea with 1 U/μl RNase T_1 (Calbiochem). After 1.5 hr at 50°C, 20 μl proteinase K mix (50 mM EDTA, 0.5% SDS, 6 mg/ml proteinase K) was added, and incubation was continued at 50°C for 15 min. The reactions were then diluted with 4 volumes of TE, PCA extracted, and ethanol precipitated. Samples dissolved in urea loading dye (7 M urea, 2.5 mM EDTA, 0.5× TBE, 0.15 mg/ml xylene cyanole, and 0.3 mg/ml bromophenol blue) were resolved by 20% denaturing PAGE.

Alkaline Hydrolysis

An alkaline ladder was generated by treating a 5′-end labeled composite snoRNA in hydrolysis buffer (60 mM sodium bicarbonate [pH 9.2], 0.5 mM EDTA, 0.3 mg/ml tRNA) at 95°C for 7 min. The reaction was diluted on ice with 5 μl formamide loading dyes (85% ultrapure formamide, 0.2× TBE, 10 mM EDTA, 0.05% bromophenol blue, and 0.05% xylene cyanole) or urea loading dyes prior to electrophoresis.

For direct analysis of in vivo 2′-*O*-methylation by partial alkaline hydrolysis, uninjected transcript RNAs and RNAs recovered from oocytes were 3′-end labeled as below. After gel purification and ethanol precipitation, the RNA was dissolved in 5 μl of hydrolysis buffer, heated at 96°C for 8 min, and diluted with 5 μl of formamide or urea loading dyes. A and G sequencing ladders were produced by treating 3′-end labeled AαS- and GαS-containing RNAs with iodine (see below).

Sequence-Specific 3′-End Labeling

Composite snoRNAs were selectively labeled using a modification of the method described by Hausner et al. [36]. For RNAs isolated from *Xenopus* GVs, the DNA oligonucleotide was IS3endG4; for uninjected transcripts the oligonucleotide was IS3trsl. These oligonucleotides anneal leaving a 5′-DNA overhang to template the incorporation of 3–4 radiolabeled dG nucleotides. For the isolated RNAs, dATP was included to extend the processed ends to a uniform length.

Total nuclear RNA or uninjected transcripts were dissolved in water and the appropriate DNA oligonucleotide (20 pmol) in a total volume of 3 μl. After heating to >90°C for 1–2 min followed by cooling for 20–25 min at room temperature, the labeling reaction was initiated by addition of 7 μl containing 1× labeling buffer (50 mM Tris-HCl [pH 7.6], 1 mM $MgCl_2$, and 1 mM DTT), 0.25–0.5 μM dATP (for isolated RNAs only), 0.5–1 μM α-^{32}P-dGTP (3000 Ci/mmol, NEN), and 19.5 U T7 Sequenase v. 2.0 (US Biochemicals). After 1 hr at 37°C, excess dGTP (200 pmol) was added, and the incubation was continued for 15 min. Reactions were diluted with an equal volume of formamide loading dyes, and the labeled RNAs were purified by 8% denaturing PAGE.

Nucleotide Analog Interference Mapping

In Vivo

For each analog-containing transcript (0.2–5 μM), 40–60 oocytes were injected with 13.9 nl each. After 4–7 hr at 18°C, GVs were isolated as described. The recovered composite snoRNA molecules were 3′-end labeled as above and, following gel purification, were dissolved in 7 μl formamide loading dye. Each sample was divided: 5 μl was added to 1 μl I_2, and 2 μl received an additional 4 μl formamide dye. To improve the resolution of the standard I_2/ethanol treatment [28], a 25 mM I_2/ethanol stock was diluted immediately prior to use to a concentration of 2 mM I_2 with formamide dye. Uninjected transcripts were 3′-end labeled and treated with iodine in parallel. After heating to >90°C for 3–4 min, RNAs were fractionated on 8%–15% sequencing gels, and the bands on dried gels were analyzed using a PhosphorImager (Molecular Dynamics). Normalized interference values (κ) were calculated as described [28].

In Vitro

Analog-containing transcripts (20 pmol, 30 μl) were treated with alkaline phosphatase (0.5 U, Roche) for 30 min at 37°C in 50 mM Tris-HCl (pH 8.5) and 0.1 mM EDTA. After enzyme inactivation at 90°C for 3–4 min, dilution with 3 volumes of TE, PCA extraction, and ethanol precipitation, the free 5′-hydroxyls were phosphorylated with γ-ATP (150 μCi, 6000 Ci/mmol, NEN) and T4 polynucleotide kinase (3 U, US Biochemicals) at 37°C for 30 min in 10 μl containing 50 mM Tris-HCl (pH 8.0), 10 mM $MgCl_2$, and 2.5 mM DTT. Following gel purification and ethanol precipitation, the RNAs were dissolved in sterile H_2O to give stock solutions of 0.5–1 × 10^6 cpm/μl. Gel shift selections were performed with 117 nM h15.5 kD, which shifted roughly 50% of the free RNA into a discrete RNP band. The excised bands were eluted into 9 mM Tris-Cl (pH 7.6), 0.9 mM EDTA, 0.27 mM NaCl, and 0.45% SDS overnight at room temperature. Following PCA extraction and ethanol precipitation, the recovered RNAs were treated in parallel with unselected RNAs with iodine and analyzed. Because the in-vivo-selected RNAs were labeled at their 3′ ends while those from in vitro selection were 5′-end labeled, the sequences appear in reverse orientation.

Gel Mobility Shift Assays

Gel mobility shift assays were performed with modifications as described [22, 23]. RNAs, internally labeled or 5′-end labeled for NAIM experiments, were preheated to 90°C for 1 min and then allowed to cool by placing the heat block on a benchtop for 15 min. The preheated RNA (1 μl) was added to 8 μl containing tRNA (1 mg/ml) and buffer A (20 mM HEPES [pH 7.9], 150 mM KCl, 1.5 mM $MgCl_2$, 0.2 mM EDTA, and 0.1% Triton X-100). Appropriate dilutions of h15.5 kD (1 μl) in buffer D were added to initiate the binding reaction (10 μl total volume). After 1 hr at 4°C, glycerol was added to 8.3% and the samples were loaded immediately onto 8% (80:1 acrylamide:bisacrylamide) nondenaturing gels (prerun for 30 min at 23.3 V/cm) in 0.5× TBE. Dried gels were analyzed using a PhosphorImager. The fraction RNA bound (RNP) was calculated as the ratio of counts in the RNP band relative to the total (RNP + free RNA). The apparent K_d (130 ± 13 nM) was determined using the equation $K_d = (RNP_{max} \times [protein])/([protein] + K_d)$, where RNP_{max} represents the maximal fraction of bound RNA and K_d is the apparent dissociation constant.

RNA Ligations

Site-specific purine substitutions in boxes D′ (A58) and D (A89) were made by three- and two-piece DNA-mediated RNA ligations, respectively [41]. The "wild-type" sequences (A at 58 and 89) were also generated by ligation. A template for transcription of nucleotides 1–44 (used for substitution in box D′) was amplified from plasmid LBW-V-37/5 (1 ng) with primers 2651/70 and 24-44Ssp using Pfu polymerase (Stratagene) with annealing at 52°C. The template for making the 5′ end (1–85) for the box D substitutions was generated by amplification of LBW-V-37/5 with primers 2651/70 and 4/e 63-85 with annealing at 56°C. After transcription by T7 RNAP, RNAs 1–44 and 1–85 were gel purified, eluted, precipitated, dissolved in water, and their concentrations were determined spectrophotometrically. RNA oligonucleotides containing the functional group substitutions and the wild-type controls were 5′-end labeled as above.

The three-piece ligation to produce box D′ substitutions was performed in two stages. The 5′ end 1–44 (40 pmol), 5′-^{32}P-A58 or A58Pur (20 pmol) and the DNA splint, 4/e sp-pro (20 pmol), were annealed by heating to 90°C for 1 min and then cooling for 15 min in 5 μl buffer containing 150 mM Tris-HCl (pH 7.6) and 60 mM KCl. The annealed RNA-DNA hybrids were added to reactions containing 50 mM Tris-HCl (pH 7.6), 10 mM $MgCl_2$, 1 mM ATP, 1% polyvinyl alcohol, 20 mM DTT, 20 U RNase Inhibitor (Roche), and 1 U T4 DNA ligase (Roche) in 10 μl. The reactions were incubated at 37°C for 2 hr, then diluted to 200 μl with TE and PCA extracted. The aqueous layer was mixed with 20 pmol of 5′-^{32}P-4/e 73-99 (pellet from ethanol

precipitation after 5′-end labeling) and ethanol precipitated. The pellet was redissolved in 5 μl containing Tris-Cl and KCl as above, and annealing and ligation steps were repeated. After incubation at 37°C for 3 hr, 1 U of RQI DNase (Promega) was added, and the incubation was continued for 15 min. The reaction was quenched by addition of 15 μl formamide dyes, and the product was gel purified. For the two-piece ligations to produce substitutions in box D, only one round of ligation was required. The ligated RNAs were dissolved in 10 μl of 1× transcription buffer and digested with RQI DNase. The DNase step was essential because the splint (4/e sppro) base pairs along the full length of the RNA.

Acknowledgments

The authors thank Niamh Cahill, Mei-Di Shu, and Yingqun Huang for performing frog surgeries; Anne Kosek for HPLC purification of phosphorothioate S_P isomers; Kazio Tycowski, Niamh Cahill, and Tets Hirose for snoRNA clones, discussions, and comments on the manuscript; Dan Klein and Martin Schmeing for helpful discussions; Tom Cech for insightful comments; and Alex Szewczak for Figure 7B and for critical reading of the manuscript. L.B.W.S. was funded by NIH fellowship GM 19683. S.A.S. was supported by NSF grant CHE-0100057. J.A.S. is an investigator of the Howard Hughes Medical Institute and recipient of NIH grant GM 26154.

Received: July 30, 2002
Revised: September 9, 2002
Accepted: September 9, 2002

References

1. Maden, B.E.H. (1990). The numerous modified nucleotides in eukaryotic ribosomal RNA. Prog. Nucleic Acid Res. Mol. Biol. *39*, 241–303.
2. Kiss-László, Z., Henry, Y., Bachellerie, J.-P., Caizergues-Ferrer, M., and Kiss, T. (1996). Site-specific ribose methylation of preribosomal RNA: A novel function for small nucleolar RNAs. Cell *85*, 1077–1088.
3. Nicoloso, M., Qu, L.-H., Michot, B., and Bachellerie, J.-P. (1996). Intron-encoded, antisense small nucleolar RNAs: The characterization of nine novel species points to their direct role as guides for the 2′-*O*-ribose methylation of rRNAs. J. Mol. Biol. *260*, 178–195.
4. Tycowski, K.T., Smith, C.M., Shu, M.-D., and Steitz, J.A. (1996). A small nucleolar RNA requirement for site-specific ribose methylation of rRNA in *Xenopus*. Proc. Natl. Acad. Sci. USA *93*, 14480–14485.
5. Tollervey, D., and Kiss, T. (1997). Function and synthesis of small nucleolar RNAs. Curr. Opin. Cell Biol. *9*, 337–342.
6. Weinstein, L.B., and Steitz, J.A. (1999). Guided tours: from precursor snoRNA to functional snoRNP. Curr. Opin. Cell Biol. *11*, 378–384.
7. Ganot, P., Jady, B.E., Bortolin, M.L., Darzacq, X., and Kiss, T. (1999). Nucleolar factors direct the 2′-*O*-ribose methylation and pseudouridylation of U6 spliceosomal RNA. Mol. Cell. Biol. *19*, 6906–6917.
8. Tycowski, K.T., You, Z.-H., Graham, P.J., and Steitz, J.A. (1998). Modification of U6 spliceosomal RNA is guided by other small RNAs. Mol. Cell *2*, 629–638.
9. Jady, B.E., and Kiss, T. (2001). A small nucleolar guide RNA functions both in 2′-*O*-ribose methylation and pseudouridylation of the U5 spliceosomal RNA. EMBO J. *20*, 541–551.
10. Gaspin, C., Cavaille, J., Erauso, G., and Bachellerie, J.P. (2000). Archaeal homologs of eukaryotic methylation guide small nucleolar RNAs: lessons from the *Pyrococcus* genomes. J. Mol. Biol. *297*, 895–906.
11. Omer, A.D., Lowe, T.M., Russell, A.G., Ebhardt, H., Eddy, S.R., and Dennis, P.P. (2000). Homologs of small nucleolar RNAs in Archaea. Science *288*, 517–522.
12. Maxwell, E.S., and Fournier, M.J. (1995). The small nucleolar RNAs. Annu. Rev. Biochem. *35*, 897–934.
13. Hüttenhofer, A., Kiefmann, M., Meier-Ewert, S., O'Brien, J., Lehrach, H., Bachellerie, J.-P., and Brosius, J. (2001). RNomics: an experimental approach that identifies 201 candidates for novel, small, non-messenger RNAs in mouse. EMBO J. *20*, 2943–2953.
14. Xia, L., Watkins, N.J., and Maxwell, E.S. (1997). Identification of specific nucleotide sequences and structural elements required for intronic U14 snoRNA processing. RNA *3*, 17–26.
15. Terns, M.P., and Terns, R.M. (2002). Small nucleolar RNAs: Versatile trans-acting molecules of ancient evolutionary origin. Gene Expr. *10*, 17–39.
16. Niewmierzycka, A., and Clarke, S. (1999). *S*-Adenosylmethionine-dependent methylation in *Saccharomyces cerevisiae*. Identification of a novel protein arginine methyltransferase. J. Biol. Chem. *274*, 814–824.
17. Omer, A.D., Ziesche, S., Ebhardt, H., and Dennis, P.P. (2002). *In vitro* reconstitution and activity of a C/D box methylation guide ribonucleoprotein complex. Proc. Natl. Acad. Sci. USA *99*, 5289–5294.
18. Tollervey, D., Lehtonen, H., Jansen, R., Kern, H., and Hurt, E.C. (1993). Temperature-sensitive mutations demonstrate roles for yeast fibrillarin in pre-rRNA processing, pre-rRNA methylation, and ribosome assembly. Cell *72*, 443–457.
19. Wang, H., Boisvert, D., Kim, K.K., Kim, R., and Kim, S.H. (2000). Crystal structure of a fibrillarin homologue from *Methanococcus jannaschii*, a hyperthermophile, at 1.6Å resolution. EMBO J. *19*, 317–323.
20. Venema, J., and Tollervey, D. (1999). Ribosome synthesis in *Saccharomyces cerevisiae*. Annu. Rev. Genet. *33*, 261–311.
21. Watkins, N.J., Gottschalk, A., Neubauer, G., Kastner, B., Fabrizio, P., Mann, M., and Lührmann, R. (1998). Cbf5p, a potential pseudouridine synthase, and Nhp2p, a putative RNA-binding protein, are present together with Gar1p in all H box/ACA-motif snoRNPs and constitute a common bipartite structure. RNA *4*, 1549–1568.
22. Nottrott, S., Hartmuth, K., Fabrizio, P., Urlaub, H., Vidovic, I., Ficner, R., and Lührmann, R. (1999). Functional interaction of a novel 15.5kD [U4/U6.U5] tri-snRNP protein with the 5′ stem-loop of U4 snRNA. EMBO J. *18*, 6119–6133.
23. Watkins, N.J., Ségault, V., Charpentier, B., Nottrott, S., Fabrizio, P., Bachi, A., Wilm, M., Rosbash, M., Branlant, C., and Lührmann, R. (2000). A common core RNP structure shared between the small nucleolar box C/D RNPs and the spliceosomal U4 snRNP. Cell *103*, 457–466.
24. Will, C.L., and Lührmann, R. (2001). Spliceosomal UsnRNP biogenesis, structure and function. Curr. Opin. Cell Biol. *13*, 290–301.
25. Vidovic, I., Nottrott, S., Hartmuth, K., Lührmannn, R., and Ficner, R. (2000). Crystal structure of the spliceosomal 15.5kD protein bound to a U4 snRNA fragment. Mol. Cell *6*, 1331–1342.
26. Klein, D.J., Schmeing, T.M., Moore, P.B., and Steitz, T.A. (2001). The kink-turn: a new RNA secondary structure motif. EMBO J. *20*, 4214–4221.
27. Winkler, W.C., Grundy, F., Murphy, B.A., and Henkin, T.M. (2001). The GA motif: An RNA element common to bacterial antitermination systems, rRNA, and eukaryotic RNAs. RNA *7*, 1165–1172.
28. Ryder, S.P., Ortoleva-Donnelly, L., Kosek, A.B., and Strobel, S.A. (2000). Chemical probing of RNA by nucleotide analog interference mapping. Methods Enzymol. *317*, 92–109.
29. Ryder, S.P., and Strobel, S.A. (1999). Nucleotide analog interference mapping of the hairpin ribozyme: implications for secondary and tertiary structure formation. J. Mol. Biol. *291*, 295–311.
30. Caffarelli, E., Fatica, A., Prislei, S., De Gregorio, E., Fragapane, P., and Bozzoni, I. (1996). Processing of the intron-encoded U16 and U18 snoRNAs: the conserved C and D boxes control both the processing reaction and the stability of the mature snoRNA. EMBO J. *15*, 1121–1131.
31. Peculis, B.A., and Steitz, J.A. (1994). Sequence and structural elements critical for U8 snRNP function in *Xenopus* oocytes are evolutionarily conserved. Genes Dev. *8*, 2241–2255.
32. Caffarelli, E., Losito, M., Giorgi, C., Fatica, A., and Bozzoni, I. (1998). *In vivo* identification of nuclear factors interacting with the conserved elements of box C/D small nucleolar RNAs. Mol. Cell. Biol. *18*, 1023–1028.
33. Lafontaine, D.L., and Tollervey, D. (2000). Synthesis and assembly of the box C+D small nucleolar RNPs. Mol. Cell. Biol. *20*, 2650–2659.

34. Reimer, G., Pollard, K.M., Penning, C.A., Ochs, R.L., Lischwe, M.A., Busch, H., and Tan, E.M. (1987). Monoclonal autoantibody from a (New Zealand black X New Zealand white)F_1 mouse and some human scleroderma sera target an M_r 34,000 nucleolar protein of the U3 RNP particle. Arthritis Rheum. *30*, 793–800.
35. Fatica, A., Galardi, S., Altieri, F., and Bozzoni, I. (2000). Fibrillarin binds directly and specifically to U16 box C/D snoRNA. RNA *6*, 88–95.
36. Hausner, T.P., Giglio, L.M., and Weiner, A.M. (1990). Evidence for base-pairing between mammalian U2 and U6 small nuclear ribonucleoprotein particles. Genes Dev. *4*, 2146–2156.
37. Cavaillé, J., and Bachellerie, J.-P. (1998). SnoRNA-guided ribose methylation of rRNA: structural features of the guide RNA duplex influencing the extent of the reaction. Nucleic Acids Res. *26*, 1576–1587.
38. Sousa, R., and Padilla, R. (1995). A mutant T7 RNA polymerase as a DNA polymerase. EMBO J. *14*, 4609–4621.
39. Kuhn, J.F., Tran, E.J., and Maxwell, E.S. (2002). Archaeal ribosomal protein L7 is a functional homolog of the eukaryotic 15.5kD/Snu13p snoRNP core protein. Nucleic Acids Res. *30*, 931–941.
40. Smith, C.M., and Steitz, J.A. (1998). Classification of *gas5* as a multi-small-nucleolar-RNA (snoRNA) host gene and a member of the 5′-terminal oligopyrimidine gene family reveals common features of snoRNA host genes. Mol. Cell. Biol. *18*, 6897–6909.
41. Moore, M.J., and Sharp, P.A. (1992). Site-specific modification of pre-mRNA: The 2'-hydroxyl groups at the splice sites. Science *256*, 992–997.
42. Kiss-László, Z., Henry, Y., and Kiss, T. (1998). Sequence and structural elements of methylation guide snoRNAs essential for site-specific ribose methylation of pre-rRNA. EMBO J. *17*, 797–807.
43. Cahill, N.M., Friend, K., Speckman, W., Li, Z.-H., Terns, R.M., Terns, M.P., and Steitz, J.A. (2002). Site-specific crosslinking analyses reveal an asymmetric protein distribution for a box C/D snoRNP. EMBO J. *21*, 3816–3828.
44. SantaLucia, J., Jr., Kierzek, R., and Turner, D.H. (1991). Functional group substitutions as probes of hydrogen bonding between GA mismatches in RNA internal loops. J. Am. Chem. Soc. *113*, 4313–4322.
45. Frey, P.A., and Sammons, R.D. (1985). Bond order and charge localization in nucleoside phosphorothioates. Science *228*, 541–545.
46. Cavaillé, J., and Bachellerie, J.P. (1996). Processing of fibrillarin-associated snoRNAs from pre-mRNA introns: An exonucleolytic process exclusively directed by the common stem-box terminal structure. Biochimie *78*, 443–456.
47. Filippini, D., Bozzoni, I., and Caffarelli, E. (2000). p62, a novel *Xenopus laevis* component of box C/D snoRNPs. RNA *6*, 391–401.
48. Romero, M.F., Kanai, Y., Gunshin, H., and Hediger, M.A. (1998). Expression cloning using *Xenopus laevis* oocytes. Methods Enzymol. *296*, 17–52.
49. Gall, J.G., Murphy, C., Callan, H.G., and Wu, Z. (1991). Lampbrush Chromosomes. In *Xenopus laevis*: Practical Uses in Cell and Molecular Biology, B.K. Kay and H.B. Peng. eds. (San Diego, CA: Academic Press, Inc.), pp. 149–166.
50. Hamm, J., Dathan, N.A., and Mattaj, I.W. (1989). Functional analysis of mutant *Xenopus* U2 snRNAs. EMBO J. *59*, 159–169.